High quality AlN for deep UV photodetectors

S. Nikishin,[1,a)] B. Borisov,[1] M. Pandikunta,[1] R. Dahal,[1,b)] J. Y. Lin,[1] H. X. Jiang,[1] H. Harris,[2] and M. Holtz[3]
[1]*Department of Electrical and Computer Engineering and Nano Tech Center, Texas Tech University, Lubbock, Texas 79409, USA*
[2]*Department of Electrical and Computer Engineering, Texas A&M University, College Station, Texas 77843, USA*
[3]*Department of Physics and Nano Tech Center, Texas Tech University, Lubbock, Texas 79409, USA*

(Received 2 May 2009; accepted 15 July 2009; published online 6 August 2009)

We have prepared large-area, 0.50×0.55 mm^2, metal-semiconductor-metal photodetectors based on AlN layers with different density of inversion domains (IDs). AlN layers were grown on (0001) sapphire substrates using gas source molecular beam epitaxy. The introduction of AlN/GaN short period superlattices after growth of AlN nucleation layer yields significant reduction in the ID density. Photodetectors with ID density of 10^6 cm^{-2} exhibit a very low dark current of 0.5 fA at zero bias, which remains below 50 fA up to a bias of ± 30 V. The peak responsivity of 0.08 A/W was obtained at a wavelength of ~202 nm. © *2009 American Institute of Physics*.
[DOI: 10.1063/1.3200229]

The optical and electrical properties of AlGaN based deep UV light emitting diodes and photodetectors (PDs) grown on a *c*-plane sapphire are very sensitive to the material quality. It is well known that high density of threading dislocation (TDs) and inversion domains (IDs) with *N*-polarity yields significant reduction in the performance of III-nitride based devices.[1–3] To improve crystal quality, initial growth generally begins with an AlN nucleation/buffer layer and often incorporates an AlGaN superlattice for blocking extended defects in thin layers.[4] Thick AlN (Ref. 5) is very attractive for fabricating metal-semiconductor-metal (MSM) PDs due to the relative simplicity of forming high quality Schottky contacts. Recently, Li *et al.* demonstrated MSM PDs, based on metal organic chemical vapor deposition (MOCVD) grown AlN on a *c*-sapphire, with peak responsivity at 200 nm.[5] Pantha *et al.*[6] observed a strong correlation between both the dark current and sensitivity of MSM PDs with the TD density in MOCVD AlN. The influence of IDs on optoelectronic properties of AlN based MSM PDs, however, is not yet understood.

In this paper, we report influence of growth conditions during gas source molecular beam epitaxy (GSMBE) with ammonia on structural and morphological properties of AlN. The material quality of the AlN epitaxial layers was studied using reflection high-energy electron diffraction (RHEED) carried out *in situ* during growth and *ex situ* using atomic force microscopy (AFM), x-ray diffraction (XRD), scanning electron microscopy (SEM) and transmission electron microscopy (TEM). The *I-V* and photoresponse characteristics of AlN-MSM-PDs are presented and discussed.

We began by investigating the effectiveness of sapphire nitridation under different conditions and the impact of nitridation on the surface morphology and crystal perfection of subsequently grown AlN layers. We found that nitridation at high ammonia flux yields the smallest root mean square (rms) roughness and best crystal perfection. Based on these results, all substrates were subsequently nitridated at 930 °C for 20 min using 115 SCCM (SCCM denotes cubic centimeters per minute at STP) ammonia flux. The onset of epitaxial growth was three dimensional (3D). AlN films are grown at a substrate temperature of 900 °C and ammonia flux of 12 SCCM with growth rate of ~200 nm/h.[7] We observed 1×1 streaky RHEED pattern (not shown here) corresponding to a two dimensional growth mode after deposition of ~10–20 nm thick AlN. Streaky 2×2 RHEED pattern corresponding to Al-polar surface[8] was observed at room temperature.

AFM images of two samples grown in the step-flow mode under the above conditions, with thicknesses of 150 and 500 nm, are shown in Figs. 1(a) and 1(b), respectively. The step height ranges from 0.5 to 1.0 nm for the thin layer and from 2.0 to 3.0 nm for the thick AlN, and the corresponding step width increases from 0.5 to 1.0 to 2.0–2.5 μm. The large-area rms roughness is 0.45 nm for a 150 nm thick layer and increases to 0.75 nm for a 500 nm thick AlN.

We note in Figs. 1(a) and 1(b) the presence of small bright spots. The 5×5 μm^2 3D AFM image of the as-grown 500 nm thick AlN (sample A) [Fig. 2(a)] reveals these spots to be columnar in shape. SEM images support this conclusion. The density of these features is lower on thicker samples. Upon etching these samples in 1:1 H_2O:KOH solution at 80 °C for 30 s, the columnar structures are removed and we observe deep pits with well defined hexagonal shapes, as shown in Fig. 2(b). We conclude that the columns possess *N*-polarity surrounded by Al polar material, signifying the presence of *N*-polar IDs. The corresponding ID density for the 500 nm thick samples is $\sim 5 \times 10^7$ cm^{-2} and is larger by a factor of ~3 for the 150 nm layers. TEM measurements, not shown here, verify that the IDs originate from the sapphire/AlN interface.

To reduce the ID density, we incorporated two AlN/GaN short period superlattices (SPSLs) into our structure with barrier and well thicknesses of ~2.0 and ~0.5 nm, respectively. For our MSM structure on sapphire substrates, a

a)Author to whom correspondence should be addressed. Electronic mail: sergey.a.nikishin@ttu.edu.
b)Also at: Department of Physics, Kansas State University, Manhattan, KS 66506-2601.

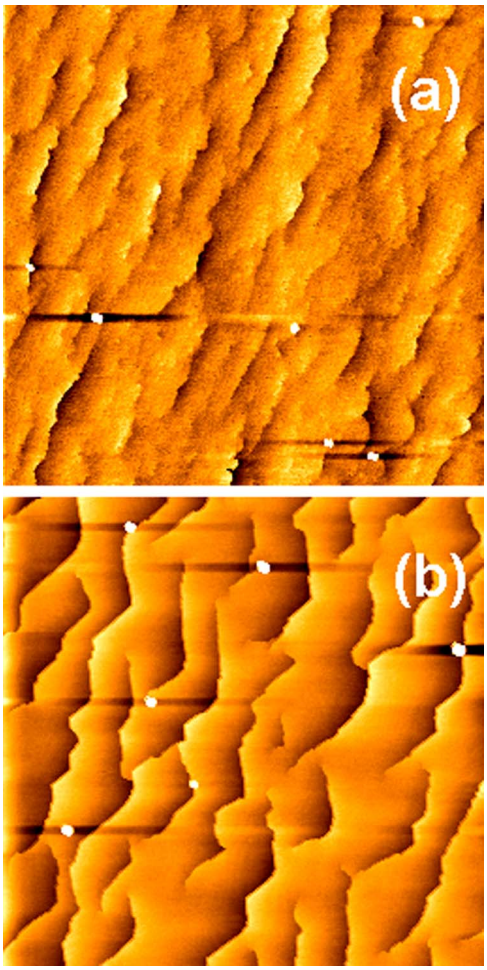

FIG. 1. (Color online) AFM image of AlN layers grown in optimized conditions: (a) 150 nm thick 5×5 μm^2 area and (b) 500 nm thick 10×10 μm^2 area.

15 nm thick nucleation AlN layer was first grown in 3D mode. Next, a 15-period SPSL is grown, followed by a 60 nm thick AlN and a 10-period SPSL. The final 500 nm thick AlN was then grown. The AFM image of 10×10 μm^2 area of this sample without IDs (sample B) is shown in Fig. 2(c). The ID density, $\sim1\times10^6$ cm^{-2}, estimated from larger AFM images, not shown, was reduced by over one order of magnitude than that in AlN layers grown without SPSLs. The results of AFM and XRD measurements are summarized in Table I.

Crystal properties have been investigated by XRD. Screw dislocation densities N_S were calculated from the full width at half maximum (FWHM) of (0002) reflection using[9–11]

$$N_S = \frac{\beta^2(0002)}{2\pi \ln 2 \times b^2}, \tag{1}$$

where b is the length of Burger vector and β is the FWHM of (0002) ω scan. For the 500 nm thick AlN (no SPSL) and 500 nm thick (with SPSL) layers we obtain consistent N_S in the range of $(6.3–6.8)\times10^5$ cm^{-2}. Edge dislocation densities N_E were estimated based on both asymmetric and skew symmetric XRD measurements. The dependences of FWHM of $(10\bar{1}1)$, $(10\bar{1}2)$, $(10\bar{1}3)$, $(10\bar{1}5)$, and $(30\bar{3}2)$ Φ-and ω-scans on the inclination angle ϕ were used to estimate N_E. Using the approach in Refs. 11 and 12, we obtain comparable values of N_E in the range of $(8.6–9.5)\times10^{10}$ cm^{-2} for both AlN layers. It is clear that insertion of SPSLs between nucleation and top AlN layers does not strongly influence either N_S or N_E. However, the density of inversion domains in sample B incorporating SPSLs is more than one order of magnitude lower than for sample A.

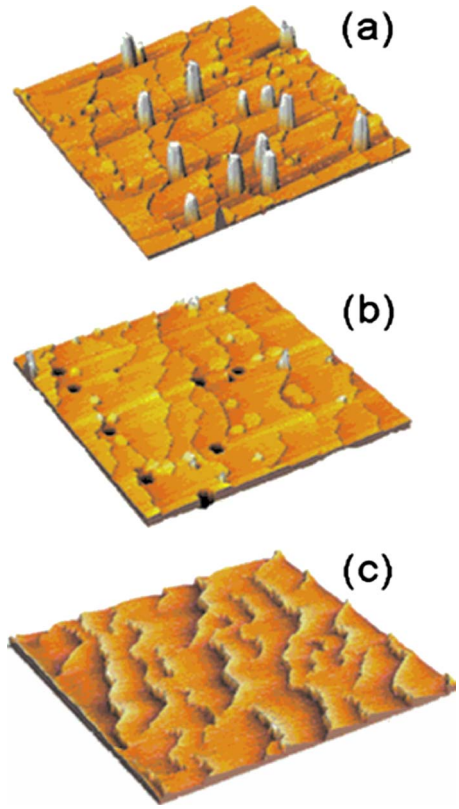

FIG. 2. (Color online) (a) AFM image (5×5 μm^2) of sample A before etching, (b) AFM image (5×5 μm^2) of the same sample after etching in KOH, and (c) AFM image (10×10 μm^2) of sample B without IDs.

These two samples were used to fabricate MSM PDs. The optical microscopy image of the detector layout is shown in Fig. 3. Active device area is 0.275 mm^2 (0.50×0.55 mm^2) and the finger electrodes width/spacing is 5 μm/5 μm. The total area of two electrodes is 0.161 mm^2. Typical *I-V* characteristic of PD fabricated on AlN with low ID density is shown in Fig. 3. Dark leakage current of $\sim$0.5 fA is measured at near zero bias. This dark current remains below 50 fA up to a bias of ±30 V. These low dark currents are the best reported for AlN large-area MSM detectors.

The PDs fabricated on AlN with high ID density demonstrated *I-V* with very low dark current similar to Fig. 3. Interestingly, the PD current remained below 20 fA even under illumination at different bias voltages, corresponding to

TABLE I. XRD results for two $\sim$500 nm thick AlN samples used for MSM PDs.

Sample	Symmetric (0002) ω FWHM (arc sec)	Screw dislocation density (cm^{-2})	Asymmetric $(10\bar{1}0)$ ω FWHM (arc sec)	Edge dislocation density (cm^{-2})	Inversion domains density (cm^{-2})
A	17.0	6.3×10^5	2952	9.5×10^{10}	5×10^7
B	17.7	6.8×10^5	2812	8.6×10^{10}	1×10^6

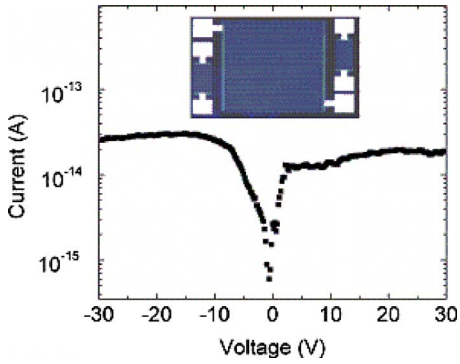

FIG. 3. (Color online) *I-V* characteristic and photograph of 0.50 $\times 0.55$ mm^2 MSM PDs.

very poor responsivity. Moreover, the response vanished completely after brief operation. The decrease in photocurrent due to illumination, or photodegradation, has been described previously and attributed to the formation of metastable defects which localize carriers.[13–15] In our case, localization is expected to involve IDs.

Spectral responsivity of PD under bias of −10 V is shown in Fig. 4. The peak responsivity of 0.08 A/W was obtained at a wavelength of ~202 nm. Cutoff at 213 nm is obtained for these devices with more than two orders of magnitude decrease in responsivity from 202 to 213 nm and more than three orders of magnitude rejection by 285 nm. We observe a weak feature seen near 310 nm (~4.0 eV) in the photoresponse in Fig. 4, at ~0.2% of the peak responsivity. Previous photoluminescence studies of MOCVD AlN reveal a broad feature near 3.9 eV, which is attributed to the presence of native defects.[16]

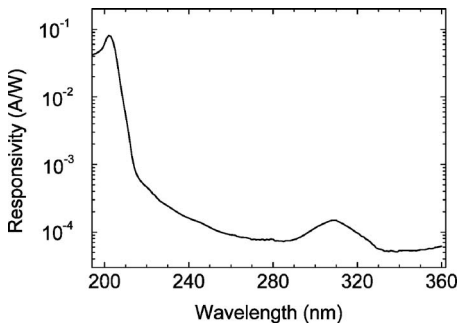

FIG. 4. Spectral response of MSM PD at −10 V bias.

In summary, high crystal quality AlN was grown by GSMBE of sapphire substrates. The introduction of AlN/GaN SPSLs reduces the density of IDs in the device AlN layers without substantially affecting the TD density. Large-area MSM solar blind PDs, with peak responsivity at 202 nm, are comparable to the state-of-the-art devices fabricated using AlN grown by MOCVD.

This work was supported in part by the National Science Foundation (Grant No. ECS-0609416), U.S. Army CERDEC contract (No. W15P7T-07-D-P040), the J. F. Maddox Foundation, and DOE (Grant No. DE-FG02-09ER46552). J.Y.L. and H.X.J. gratefully acknowledge the support of the Linda and Edward Whitacre endowment through the AT&T Foundation.

[1] S. Nakamura and G. Fasol, *The Blue Laser Diode: GaN Based Light Emitters and Lasers* (Springer, Berlin, 1997), pp. 201–215.
[2] H. Morkoç, *Nitride Semiconductors and Devices* (Springer, Berlin, 1999), Vol. 32, pp. 149–190.
[3] H. Temkin, in *Advanced Semiconductor and Organic Nano-Techniques-Part-I*, edited by H. Morkoç (Academic, San Diego, 2003), and references therein.
[4] S. A. Nikishin, N. N. Faleev, V. G. Antipov, S. Francoeur, L. Grave de Peralta, G. A. Seryogin, H. Temkin, T. I. Prokofyeva, M. Holtz, and S. N. G. Chu, Appl. Phys. Lett. **75**, 2073 (1999).
[5] J. Li, Z. Y. Fan, R. Dahal, M. L. Nakarmi, J. Y. Lin, and H. X. Jiang, Appl. Phys. Lett. **89**, 213510 (2006).
[6] B. N. Pantha, R. Dahal, M. L. Nakarmi, N. Nepal, J. Li, J. Y. Lin, H. X. Jiang, Q. S. Paduano, and D. Weyburne, Appl. Phys. Lett. **90**, 241101 (2007).
[7] X. Xu, V. Kuryatkov, B. Borisov, M. Pandikunta, S. A. Nikishin, and M. Holtz, *MRS Symposia Proceedings No. 1108* (Materials Research Society, Warrendale, PA, 2009), p. 1108-A09-34.
[8] S. A. Nikishin, B. A. Borisov, A. Chandolu, V. V. Kuryatkov, H. Temkin, M. Holtz, E. N. Mokhov, Yu. Makarov, and H. Helava, Appl. Phys. Lett. **85**, 4355 (2004).
[9] R. Chierchia, T. Böttcher, H. Heinke, S. Einfeldt, S. Figge, and D. Hommel, J. Appl. Phys. **93**, 8918 (2003).
[10] T. Metzger, R. Höpler, E. Born, O. Ambacher, M. Stutzmann, R. Stömmer, M. Schuster, H. Göbel, S. Christiansen, M. Albrecht, and H. P. Strunk, Philos. Mag. A **77**, 1013 (1998).
[11] V. M. Kaganer, O. Brandt, A. Trampert, and K. H. Ploog, Phys. Rev. B **72**, 045423 (2005).
[12] H. Heinke, V. Kirchner, S. Einfeldt, and D. Hommel, Phys. Status Solidi A **176**, 391 (1999).
[13] C. Tannous, G. Leclerc, and A. Yelon, J. Phys.: Condens. Matter **1**, 4367 (1989).
[14] K. Shimakawa, S. Inami, T. Kato, and S. R. Elliott, Phys. Rev. B **46**, 10062 (1992).
[15] N. Manikandan and S. Asokan, J. Non-Cryst. Solids **354**, 3732 (2008).
[16] K. B. Nam, M. L. Nakarmi, J. Y. Lin, and H. X. Jiang, Appl. Phys. Lett. **86**, 222108 (2005).